



# Coordination of PSS and STATCOM-POD to Improve Low-Frequency Oscillation Characteristics of Wind-Thermal-Bundled Transmission System Using Improved Salp Swarm Algorithm

Ping He<sup>1</sup> · Lei Yun<sup>1</sup> · Yukun Tao<sup>1</sup> · Jiale Fan<sup>1</sup> · Zhiwen Pan<sup>1</sup> · Mingyang Wang<sup>1</sup>

Received: 13 January 2023 / Revised: 5 August 2023 / Accepted: 15 August 2023 / Published online: 2 September 2023  
 © The Author(s) under exclusive licence to The Korean Institute of Electrical Engineers 2023

## Abstract

An approach is proposed in this paper to coordinate the power system stabilizer and static synchronous compensator with additional power oscillation damping controller (STATCOM-POD) in the wind-thermal-bundled (WTB) transmission system. An improved salp swarm algorithm is proposed. Adaptive weight factor, Levy flight disturbance strategy, non-uniform Gaussian mutation operator and greedy selection strategy are introduced to improve the leader and follower position update formula in the salp swarm algorithm (SSA). This algorithm improves the ability of SSA to avoid falling into the local optimum and can be used to coordinate and optimize controller parameters. Considering the controller's role in controlling the system voltage and damping, an objective function is built to improve the low-frequency oscillation characteristics of the WTB transmission system by comprehensively evaluating the real part and damping ratio of low-frequency oscillation mode and bus voltage. The eigenvalue analysis and time domain simulation are used to verify the effectiveness of the proposed coordination method.

**Keywords** WTB · PSS · STATCOM-POD · Coordination · ISSA · Low-frequency oscillation

## List of Symbols

$K_{PSS}$	Damping gain of PSS	$P_f, Q_f, P_z, Q_z$	Active power and reactive power generated by the stator and rotor
$T_{PSS}$	Wash out time constant of PSS	$P_b, Q_b, P_s, Q_s$	Active power and reactive power absorbed from the grid by the grid side converter and injected into the grid by the doubly fed wind turbine
$T_{p1}, T_{p2}, T_{p3}, T_{p4}$	Lead-lag time constants of PSS	$V_i, V_r$	Measured voltage of the node and reference voltage
$v_m$	Wind speed	$V^{POD}$	POD output signal
$\beta, \beta_r$	Pitch angle and reference value of pitch angle	$K_c, T_c$	Gain and time constant of STATCOM voltage regulator
$T_m, T_e$	Output of the mechanical torque by the fan and the mechanical electromagnetic torque of the generator rotor	$i_{SH}, \dot{i}_{SH}$	Injected current of STATCOM node and:the first order differential of $i_{SH}$
$\omega_v, \omega_s$	Fan angular velocity and generator angular speed	$K_p$	Magnification of POD
$\theta_s$	Generator rotor angle	$T_p$	Time constant of the isolated link of POD
		$T_1, T_2, T_3, T_4$	Lead-lag time constants of POD

✉ Ping He  
 hplkz@126.com

<sup>1</sup> College of Electrical and Information Engineering, Zhengzhou University of Light Industry, Zhengzhou 450002, Henan Province, China

$\Delta \mathbf{x}_r, \Delta \mathbf{x}_s$	Vector of the state variable of the synchronous unit in the receiving end system and related to WTB system and its control system	$x_j^k$	$j$ th variable value of the location of the $k$ th salp(follower)
$A_s, B_s, A_r, B_r, C_1-F_1, C_2-F_2$	Coefficients multiplied by each variable	$\sigma$	Standard deviation of Gaussian distribution
$\lambda_i$	$i$ th eigenvalue of the state matrix $A$	$X(t)$	Original position (the position after $t$ th iteration)
$I$	Identity matrix with the same order as matrix $A$	$X^*(t)$	New position after greedy selection strategy is used
$\delta_i, \beta_i$	Real part and imaginary part corresponding to the $i$ th eigenvalue	$X(t+1)$	Position after $(t+1)$ th iteration
$P_{ij}$	Participation factor of the $i$ th state variable to the $j$ th eigenvalue	<b>Abbreviations</b>	
$\phi, \psi$	Left and right eigenvector of the state matrix $A$	PSS	Power system stabilizer
$\sigma_i, \xi_i$	Real part and damping ratio of the $i$ th low frequency oscillation mode of the system	STATCOM-POD	Static synchronous compensator with additional power oscillation damping controller
$\alpha, \beta_s$	Weight coefficients	WTB	Wind-thermal-bundled
$\sigma_0, \xi_0$	Expected real part and expected damping ratio of characteristic value	ISSA	Improved salp swarm algorithm
$V_j(t), V_j(0)$	Voltage amplitude and voltage before fault of the $j$ th node	SSA	Salp swarm algorithm
$V_{jmin}$	Minimum voltage of the $j$ th node	SVC	Static var compensator
$n$	Number of observation nodes	FACTS	Flexible alternative current transmission systems
$t_0, t_e$	End time of fault and simulation	DFIG	Double fed induction generator
$w_1, w_2$	Weighting coefficients	WTGS	Wind turbine generator systems
$C_1, C_2$	Weighting coefficients	AC	Alternative current
$l, L$	Current and maximum number of iteration	SG	Synchronous generator
$w_{max}, w_{min}$	The maximum and minimum value of inertia weight	<b>1 Introduction</b>	
$s$	Levy motion step	The use of fossil energy is a major source of global greenhouse gas emissions. The use of renewable energy can reduce greenhouse gas emissions and mitigate climate change [1, 2]. The rapid development of wind energy facilitates the shift of the global energy system to a high percentage of renewable energy system. According to the distribution of power resources and loads, wind-thermal-bundled(WTB) transmission has become an important way of power transmission in the new energy base [3, 4]. Under this transmission mode, the interaction between power supply and power grid is particularly complex and low-frequency oscillation may be caused due to insufficient damping when disturbed [5, 6]. Therefore, it is of great significance to improve the damping characteristics of the WTB transmission system.	
$\mu, v$	Random numbers with normal distribution	An auxiliary control signal for excitation system of synchronous generator (SG) can be provided by power system stabilizer(PSS) to suppress low-frequency oscillation and	
$x_j^i, F_j$	$j$ th variable value of the location of the $i$ th salp (leader) and the food location		
$ub_j, lb_j$	Upper and lower limit of the $j$ th variable		

improve overall stability of power system [7–9]. However, the use of PSSs sometimes can not provide sufficient damping for inter regional oscillations. In the system with wind power, the use of PSSs also causes the changes of the voltage curve, resulting in the reduction of voltage stability [10–12]. In the system with wind power, in order to improve the voltage stability, reactive power compensation devices are usually applied in the system. Because the response time of the static synchronous compensator (STATCOM) is fast, the device is usually applied in the system to solve the voltage stability problem [13–15]. The damping of inter region oscillation mode can be enhanced by adding power oscillation damping controller to STATCOM [16]. However, studies have shown that interaction effect would appear among different controllers when they coexist in power system, that is, once inappropriate setting for controller parameters exists, different types of controllers may deteriorate system damping, and even increase oscillation [17, 18]. In order to solve this problem, it is necessary to coordinate and optimize the controller parameters. A few researches are made along that line. Reference [19] introduce Cuckoo Search (CS) algorithm for optimal PSSs design in a multimachine power system. Simulation results confirm the robustness and superiority of the optimized controllers in providing good damping characteristic to system oscillations over a wide range of loading conditions. Reference [20] uses particle swarm optimization algorithm to coordinate PSS and static var compensator (SVC) controllers, which improves the stability of power system. Reference [21] uses the salp swarm algorithm (SSA) to coordinate and optimize the parameters of PSS and flexible alternative current transmission systems (FACTS) controllers to improve the stability of power system. The SSA is a meta-heuristic algorithm. Compared with whale optimization algorithm, particle swarm optimization, simulated annealing, crow search algorithm, butterfly optimization algorithm and other traditional optimization algorithms, salp swarm algorithm has the advantages of fewer parameters, simple structure, easy implementation and better optimization directive [22]. But it still has the problems of low convergence accuracy in the later iteration and falling in local optimum [23].

Some studies have shown that before installing FACTS devices, the FACTS devices can be located and installed on weak buses to improve the voltage distribution and power system stability [24, 25].

Based on the above research, this paper proposes a coordinated optimization strategy of PSS and static synchronous compensator with additional power oscillation damping controller (STATCOM-POD). The purpose of this strategy is to improve the damping characteristics of WTB transmission system, and to eliminate the interaction of different controllers avoiding causing an adverse effect on the power system. Firstly, based on MATLAB, the model of WTB system is

built. The weak bus is selected by calculating the maximum load carrying capacity of each load bus, and the designed STATCOM-POD is installed on the bus. In order to solve the local optimum problem of the SSA, an improved salp swarm algorithm (ISSA) is proposed. According to the ISSA, the coordination and optimization model of PSS and STATCOM-POD controllers is constructed. Finally, the simulations of various operating conditions are carried out. Eigenvalue analysis and time domain simulation results verify the effectiveness of the proposed coordinated optimization strategy. The main contributions of this paper are as follows.

- (1) An ISSA is proposed based on adaptive weight factor, Levy flight disturbance strategy, non-uniform Gaussian mutation operator and greedy selection strategy strategies. It implements computationally an ISSA to perform the design of the PSS and STATCOM-POD controllers. The superiority in finding the minimum value for ISSA is proved compared with SSA through CEC17 test function. The ISSA has a strong ability to find optimal solution.
- (2) Based on the real part and damping ratio of low-frequency oscillation mode and bus voltage, it validates the ISSA as an optimization technique for adjusting the parameters of the PSS and STATCOM-POD controllers to improve the low-frequency oscillation characteristics of WTB transmission system.
- (3) In order to verify the applicability of the proposed coordinated control method, simulation is carried out on the large system IEEE 16-machine 68-bus. The results further verify the proposed ISSA can effectively coordinate the controller parameters.

The rest of this paper is organized as follows:

The Sect. 2 introduces the model of the WTB system, STATCOM-POD and PSS; The Sect. 3 introduces the linearization model of the WTB system; The Sect. 4 introduces the coordinated optimization strategy and proposes an ISSA; The Sect. 5 introduces the simulation results of various operating conditions on the IEEE 4-machine 2-area system and the IEEE 16-machine 68-bus system. The simulation results are analyzed in this section.

## 2 Modeling of System

### 2.1 The Model of Doubly Fed Induction Wind Turbine Generator Systems

Double fed induction generator (DFIG) is the mainstream machine model currently. The mathematical model of doubly fed induction wind turbine generator systems (WTGS) is mainly composed of wind speed model, aerodynamic model,

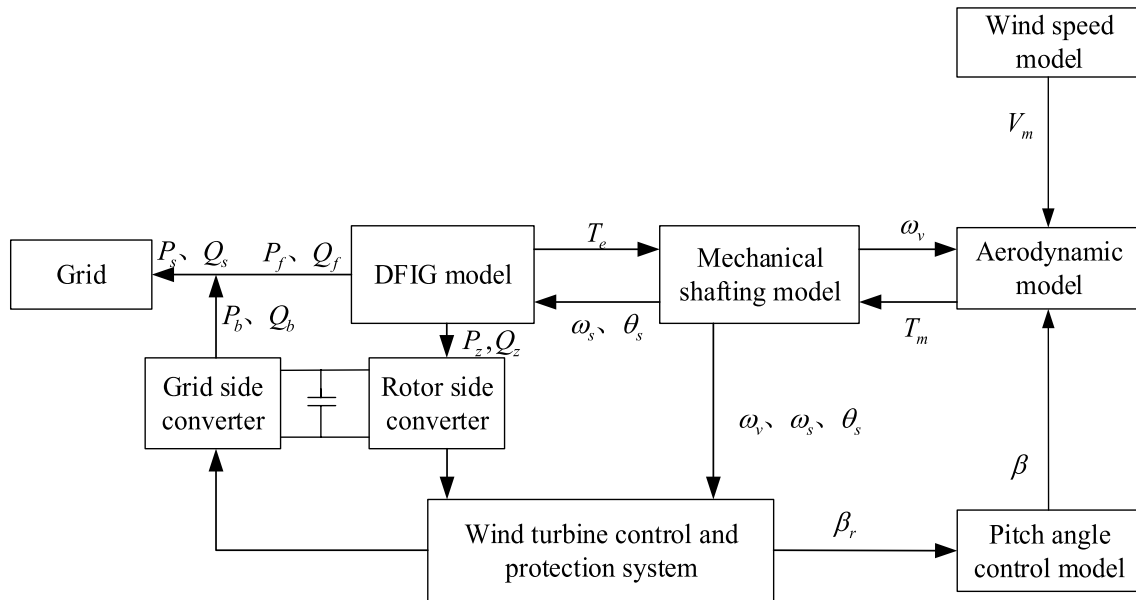


Fig. 1 The structure diagram of doubly fed induction WTGS

wind turbine shafting model, DFIG model, converters and its control system model [26], as shown in Fig. 1.

Double mass block model is adopted for fan shaft system model, and its dynamic equation and aerodynamic mathematical model of WTGS can be referred to the literature [27]. In order to ensure the stable output of wind power and its conversion efficiency, when the wind speed changes, pitch angle control strategy is employed. The adjustment equation of pitch and the fourth order mathematical model of DFIG under  $d-q$  coordinate axis can be referred to the literature [28]. The converters of doubly fed WTGS are composed of rotor side converter, grid side converter and etc. [29].

### 2.2 The Model of PSS

PSS increases the damping of low-frequency oscillation modes by providing additional signals to be applied to the auxiliary control unit of the generator excitation system, which regulates the generator excitation to improve the stability limit [30, 31]. PSS can be described by the following equation:

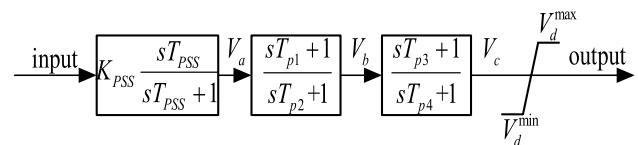


Fig. 2 The structure diagram of PSS

$$\begin{cases} \frac{dV_a}{dt} = -(K_{PSS}\omega + V_a)/T_{PSS} \\ \frac{dV_b}{dt} = \left( \left( 1 - \frac{T_{p1}}{T_{p2}} \right) (K_{PSS}\omega + V_a) - V_b \right) / T_{p2} \\ \frac{dV_c}{dt} = \left( \left( 1 - \frac{T_{p3}}{T_{p4}} \right) \left( V_b + \left( \frac{T_{p1}}{T_{p2}} (K_{PSS}\omega + V_a) \right) \right) - V_c \right) / T_{p4} \\ V_d = V_c + \frac{T_{p3}}{T_{p4}} \left( V_b + \frac{T_{p1}}{T_{p2}} (K_{PSS}\omega + V_a) \right) \end{cases} \quad (1)$$

where  $\omega$  is the generator rotor speed.

The control block diagram of PSS is shown in the Fig. 2.

where  $V_a$ ,  $V_b$  and  $V_c$  are the output signals of each link;  $V_d$  is the total output signal of the module. The input signal of PSS can select the rotor speed, active power and bus voltage amplitude of the generator. In this paper, the rotor speed of the generator is selected as the input signal.

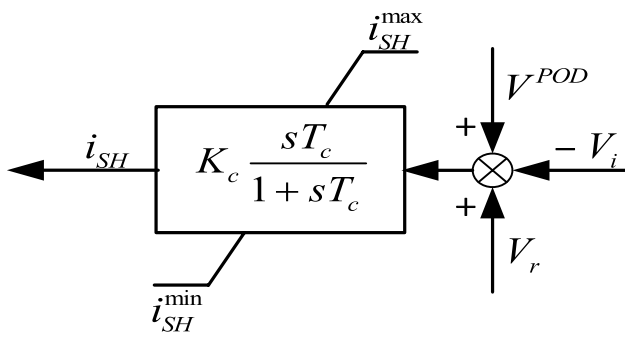


Fig. 3 Control block diagram of STATCOM

### 2.3 The Model of Static Synchronous Compensator

STATCOM is one of the shunt devices in the family of FACTS, which regulates the alternative current (AC) voltage by providing or absorbing reactive power. In this paper, STATCOM current injection model is adopted [32, 33]. The control block diagram of STATCOM is shown in the Fig. 3. STATCOM can be equivalent to a time constant regulator and has the ability to dynamically exchange reactive power with the network. The node injection current  $i_{SH}$  and injected reactive power  $Q$  can be expressed as:

$$\begin{cases} i_{SH} = (K_c(V_r + V^{POD} - V_i) - i_{SH})/T_c \\ Q = i_{SH}V_i \end{cases} \quad (2)$$

### 2.4 Additional Power Oscillation Damping Controller

When FACTS device is attached with a power oscillation damping(POD) controller, it can provide supplementary damping of low-frequency oscillation, especially for inter-regional mode oscillation. The POD designed in this paper includes amplification, isolation, phase compensation and

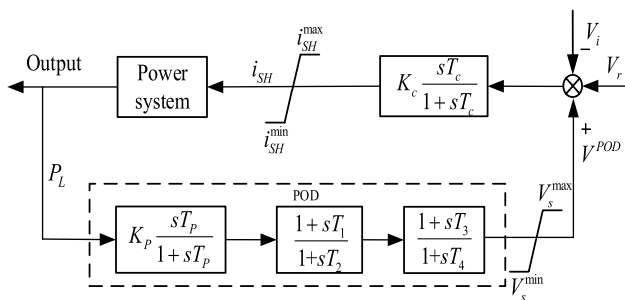


Fig. 4 The control block diagram of STATCOM-POD

amplitude limiting links. The transfer function block diagram for POD is as follows:

$$G(s) = K_p \frac{sT_p}{1 + sT_p} \frac{1 + sT_1}{1 + sT_2} \frac{1 + sT_3}{1 + sT_4} \quad (3)$$

The additional POD control enables the STATCOM to maximize the output or absorb reactive power, increase system damping, effectively suppress low-frequency oscillation, and improve system operating characteristics.

The design of STATCOM-POD control block diagram is shown in Fig. 4. An additional control signal is added to the AC voltage control part of STATCOM. In order to avoid overshoot, an amplitude limiting link is added to limit the amplitude of the regulating signal generated by the control link. The line active power, reactive power, current amplitude, voltage and etc. can be select as the POD input.

signal according to the situation. In this paper, the line active power  $P_L$  is selected as the STATCOM-POD input signal.

## 3 Linearization of System Model

By using Lyapunov stability rule and linearizing the power system model near a stable point, the linearized model of the system can be obtained. The power system connection diagram of WTB system is shown in the Fig. 5.

where  $\Delta P_s + \Delta Q_s$  is the electric energy injected into the power system by WTB transmission system;  $\Delta V_s$  and  $\Delta \varphi_s$  are respectively the magnitude and phase of the voltage at the connection between WTB transmission system and the power system;  $\Delta P_r + \Delta Q_r$  is the electric energy injected into

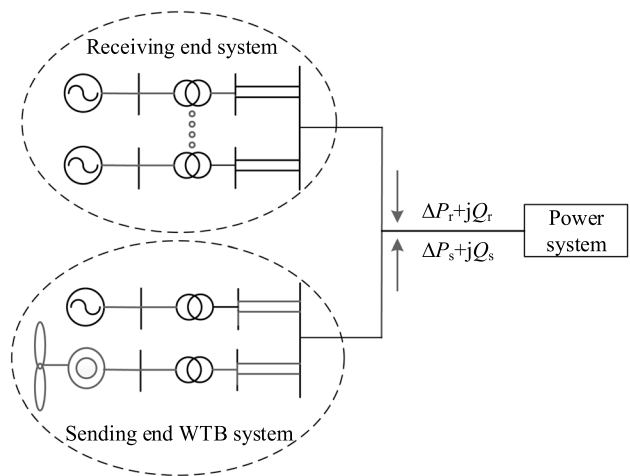


Fig. 5 The diagram of WTB transmission system

the power system by the receiving end system. The state equation of WTB transmission system can be expressed as:

$$\begin{cases} \frac{d\Delta\mathbf{x}_s}{dt} = \mathbf{A}_s\Delta\mathbf{x}_s + \mathbf{C}_1\Delta V_s + \mathbf{C}_2\Delta\varphi_s \\ \begin{bmatrix} \Delta P_s \\ \Delta Q_s \end{bmatrix} = \mathbf{B}_s\Delta\mathbf{x}_s + \mathbf{D}_1\Delta V_s + \mathbf{D}_2\Delta\varphi_s \end{cases} \quad (4)$$

$$\begin{cases} \frac{d\Delta\mathbf{x}_r}{dt} = \mathbf{A}_r\Delta\mathbf{x}_r + \mathbf{E}_1\Delta P_s + \mathbf{E}_2\Delta Q_s \\ \begin{bmatrix} \Delta V_s \\ \Delta\varphi_s \end{bmatrix} = \mathbf{B}_r\Delta\mathbf{x}_r + \mathbf{F}_1\Delta P_s + \mathbf{F}_2\Delta Q_s \end{cases} \quad (5)$$

After simplifying Eqs. (4) and (5), the state-space model of WTB transmission system can be obtained [34, 35]:

$$\frac{d}{dt} \begin{bmatrix} \Delta\mathbf{x}_s \\ \Delta\mathbf{x}_r \end{bmatrix} = \begin{bmatrix} \mathbf{A}_{s1} & \mathbf{A}_{r1} \\ \mathbf{A}_{s2} & \mathbf{A}_{r2} \end{bmatrix} \begin{bmatrix} \Delta\mathbf{x}_s \\ \Delta\mathbf{x}_r \end{bmatrix} = \mathbf{A} \begin{bmatrix} \Delta\mathbf{x}_s \\ \Delta\mathbf{x}_r \end{bmatrix} \quad (6)$$

where:

$$\begin{aligned} \mathbf{A}_{s1} &= [\mathbf{C}_1 \ \mathbf{C}_2]\mathbf{B}_r + [\mathbf{C}_1 \ \mathbf{C}_2][\mathbf{F}_1 \ \mathbf{F}_2](\mathbf{I} - [\mathbf{D}_1 \ \mathbf{D}_2][\mathbf{F}_1 \ \mathbf{F}_2])^{-1}[\mathbf{D}_1 \\ &\mathbf{D}_2]\mathbf{B}_r \\ \mathbf{A}_{r1} &= \mathbf{A}_s + [\mathbf{C}_1 \ \mathbf{C}_2][\mathbf{F}_1 \ \mathbf{F}_2](\mathbf{I} - [\mathbf{D}_1 \ \mathbf{D}_2][\mathbf{F}_1 \ \mathbf{F}_2])^{-1}\mathbf{B}_s \\ \mathbf{A}_{s2} &= \mathbf{A}_r + [\mathbf{E}_1 \ \mathbf{E}_2][\mathbf{C}_1 \ \mathbf{C}_2][\mathbf{F}_1 \ \mathbf{F}_2](\mathbf{I} - [\mathbf{D}_1 \ \mathbf{D}_2][\mathbf{F}_1 \ \mathbf{F}_2])^{-1}[\mathbf{D}_1 \\ &\mathbf{D}_2]\mathbf{B}_r \\ \mathbf{A}_{r2} &= [\mathbf{E}_1 \ \mathbf{E}_2](\mathbf{I} - [\mathbf{D}_1 \ \mathbf{D}_2][\mathbf{F}_1 \ \mathbf{F}_2])^{-1}\mathbf{B}_s \end{aligned}$$

The eigenvalue is determined according to the Eq. (7). The system eigenvalue  $\lambda_i = \delta_i + j\beta_i$  can be determined through the solution of the characteristic Eq. (7) of the state matrix  $\mathbf{A}$ .

$$\det(\mathbf{I} - \mathbf{A}) = 0 \quad (7)$$

The damping ratio can be determined according to the eigenvalue, which is given by:

$$\xi_i = \frac{-\delta_i}{\sqrt{\delta_i^2 + \beta_i^2}} \quad (8)$$

The participation factor matrix is calculated by using the left and right eigenvectors of the state matrix. The participation factor gives the relationship between state variables and the eigenvalue of the modes [36]. Its value signifies the degree of influence of a particular mode on the dynamic response of the system. The participation factor of  $i$ th mode can be defined as:

$$p_{ij} = \frac{\phi_{ij}\psi_{ij}}{\phi_i^T\psi_i} \quad (9)$$

## 4 Parameter Optimization Design Formulation

### 4.1 Optimization Objectives and Constraint Conditions

In this section, the coordination and optimization problem of PSS and STATCOM-POD controller parameters is transformed into the problem of finding the minimum value of the objective function. By coordination and optimization of parameters, the low-frequency oscillation of the system can be suppressed while the voltage stability can be guaranteed.

The principle of designing the objective function is to use damping adjustment to suppress low-frequency oscillation. The real part and damping ratio of the eigenvalue help to determine the rate of decay of oscillation. Therefore, this paper considers the size of damping ratio and real part of the eigenvalue. The objective function can be expressed as:

$$\min J_1 = \alpha \sum_{\delta_i \geq \delta_0} (\sigma_0 - \sigma_i)^2 + \beta_s \sum_{\xi_i \leq \xi_0} (\xi_0 - \xi_i)^2 \quad (10)$$

The voltage stability mainly considers two aspects. On the one hand, the amplitude of voltage oscillation in the transient process of the WTB system is considered. On the other hand, the time to recover to the stability in the transient process is considered. Then the objective function of transient voltage stability performance can be expressed as:

$$\min J_2 = w_1 \int_{t_0}^{t_e} \sum_{j=1}^n [V_j(t) - V_j(0)]^2 dt - w_2 \sum_{j=1}^n V_{j\min} \quad (11)$$

In this paper,  $w_1$  and  $w_2$  are respectively set as  $1/[n \times (t_e - t_0)]$  and 1.

Since the voltage stability and small signal stability are considered at the same time,  $J_1$  and  $J_2$  should be comprehensively considered for the optimization objective function. The established objective function is:

$$J = C_1 J_1 + C_2 J_2 \quad (12)$$

The values of  $C_1$  and  $C_2$  are determined according to the actual system structure and the severity of stability problems.

Based on the above theory, the STATCOM-POD parameter optimization problem can be expressed as:

Minimize  $J$

According to Sect. 2, STACOM-POD constraints are defined as:

$$A_{\min} \leq A \leq A_{\max}$$

PSS constraints are defined as:

$$B_{\min} \leq B \leq B_{\max}$$

where  $A$  contains the parameters to be optimized of the STATCOM-POD controller, defined as  $A = [K_p, T_p, K_c, T_c, T_1, T_2, T_3, T_4]$ ;  $A_{\max}$  and  $A_{\min}$  are the upper and lower limit of the STATCOM-POD controller parameters; The value's range of  $K_p$  and  $K_c$  is [1, 10], and the value's range of other parameters in  $A$  is [0.01, 1];  $B$  contains the parameters to be optimized of the PSS controller, defined as  $B = [K_{PSS}, T_{p1}, T_{p3}]$ ;  $B_{\max}$  and  $B_{\min}$  are the upper and lower limit of the PSS controller parameters; The value's range of  $K_{PSS}$  is [1, 10], and the value's range of other parameters in  $B$  is [0.01, 0.5] [37, 38].

## 4.2 ISSA

To solve the problem of falling into local optimum in the optimization process for SSA, this paper proposes improved methods of SSA. The leader position update formula and follower position update formula are made the following improvement respectively:

### Improvement of leader position update formula

In the leader position update phase of the SSA, individuals move around the food source, and the search scope is not limited. In the later iteration, individuals can not accurately search at the extreme point, and may even jump out of the extreme point. In addition, leaders only change their positions according to the food source. When the food falls into the local optimum, it will mislead other search agents to stagnate in the local optimum. In order to solve these problems, the improvement idea of this paper for the leader position update formula is to introduce adaptive weight factor and Levy flight strategy to update the leader position.

In the leader position update formula, parameter  $c_1$  can make the exploration and development ability of SSA in a better state, and it is the most important parameter in the SSA. The formula is as follows:

$$c_1 = 2e^{-(4t/L)^m} \quad (13)$$

The value of the power coefficient in the formula plays a vital role in the exploration and development ability of the algorithm. In SSA,  $m$  is taken as 2. But according to the conclusion in literature [39], when  $m = 2.5$ , the parameter  $c_1$  can make the exploration ability and development ability of the SSA in a better state. In this paper,  $m$  is taken as 2.5.

Aiming at the problem that SSA's search scope is not limited in the leader update stage, an adaptive weighting factor is added to multiply with food source location. The influence of the food source location on the leader gradually decreases with the increase of the number of iteration. In the early iteration, it is avoided to fall into the local extreme value, and in the late iteration, it is more and more close to the optimal value, achieving higher solution accuracy.

The formula of adaptive weight factor is as follows:

$$w = w_{\max} - (w_{\max} - w_{\min}) \times (t/L)^2 \quad (14)$$

Through many tests, the algorithm has the best performance when  $w_{\max} = 0.9$  and  $w_{\min} = 0.4$ . As the iteration progresses, the inertia weight decreases linearly from 0.9 to 0.4. At the beginning of the iteration, the larger inertia weight is, the better exploration ability of the algorithm is. At the

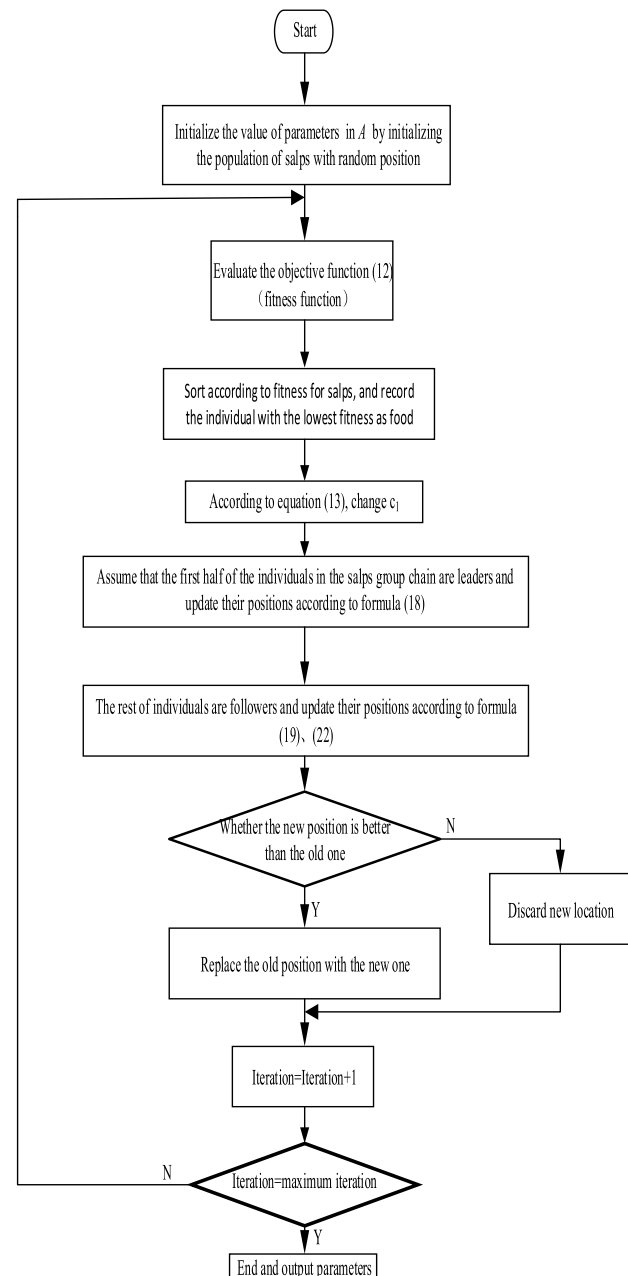
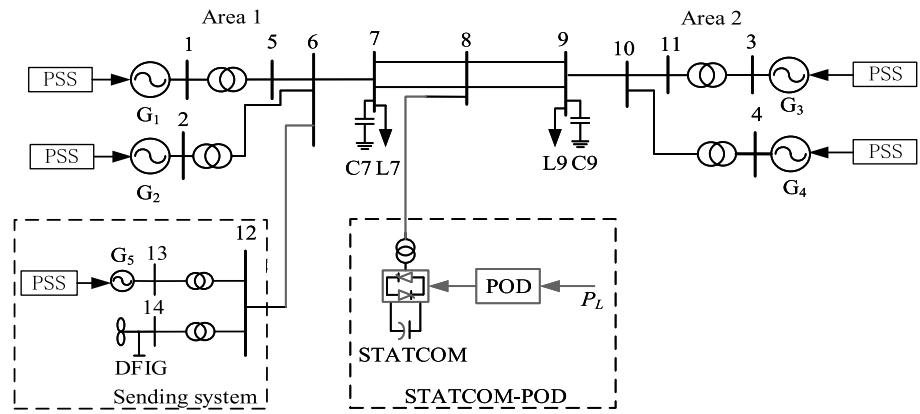


Fig. 6 Optimization flow chart

**Fig. 7** Simulation model of WTB system



late phase of the iteration, the smaller inertia weight is, the better development ability of the algorithm is.

Aiming at the problem that SSA algorithm is easy to fall into local optimum, Levy flight disturbance strategy is introduced. Levy flight is a kind of random walk strategy with occasional big steps. In optimization, this characteristic makes Levy flight especially useful for performing large jumps, which are precisely what is needed to allow a possibly stuck algorithm to escape from a local optimum and restart the search in a different region of the search space. As a global searching operator, Levy flight mechanism searches for space using short-distance walking combined with long-distance jumping routes. The long-term short-step local search in the Levy flight mechanism can improve the diversity and traversal of the algorithm. The short-term long-step global jump can make the search agents jump out of the local optimum and improve the global exploration capability [40].

The length of the motion track of Levy's flight characteristic motion is a process of random change. There is no fixed distribution function. The research summary points out that the distribution density function of Levy flight step change can be simply expressed as:

$$L(s) \sim |s|^{-1-\alpha}, \quad 0 < \alpha \leq 2 \tag{15}$$

$s$  is expressed as:

$$s = \frac{\mu}{|v|^{1/\alpha}} \tag{16}$$

where  $\mu \sim N(0, \sigma^2 \mu)$ ,  $v \sim N(0, \sigma^2 v)$ ;  $\sigma^2 \mu$  and  $\sigma^2 v$  can be obtained by (18).

$$\begin{cases} \sigma_\mu = \left\{ \frac{\Gamma(1+\gamma) \sin(\pi\gamma/2)}{\Gamma[(1+\gamma)/2] \alpha 2^{(\gamma-1)/2}} \right\}^{1/\gamma} \\ \sigma_v = 1 \end{cases} \tag{17}$$

where  $0 < \gamma < 2$ ; The value of  $\gamma$  is generally 1.5.

**Table 1** Ranking of load bus maximum load carrying capacity

Bus	$Q_{\max}(\text{p.u.})$
8	75.2
7	130.8
12	139.3
9	155.9
6	191.4
10	202.1
5	245.7
11	284.4

**Table 2** Low-frequency oscillation modes of the system

	Mode	$\lambda$	$\xi/\%$	$f/\text{Hz}$	DMs
Case1	1	$-0.5111 \pm j6.3096$	8.07	1.0042	$G_3, G_4$
	2	$-0.7932 \pm j5.6762$	13.84	0.9034	$G_1, G_2$
	3	$-0.4330 \pm j4.3622$	9.88	0.6943	$G_1, G_2, G_5$
	4	$-0.1103 \pm j3.3204$	3.32	0.5285	$G_3, G_4, G_5$
	5	$-0.2071 \pm j0.5026$	38.09	0.0800	$G_1-G_5, \text{DFIG}$
Case2	1	$-1.0256 \pm j6.4280$	15.76	1.0230	$G_3, G_4$
	2	$-1.6905 \pm j5.7188$	28.35	0.9102	$G_1, G_2$
	3	$-0.7540 \pm j4.3018$	17.26	0.6847	$G_1, G_2, G_5$
	4	$-0.2932 \pm j3.1433$	9.29	0.5003	$G_3, G_4, G_5$
	5	$-0.1714 \pm j0.5518$	29.66	0.0878	$G_1-G_5, \text{DFIG}$

Based on the above sections, the leader's position is updated according to the following formula (18):

$$x_j^i = \begin{cases} w \times F_j + c_1((ub_j - lb_j)c_2 + lb_j) \times s, & c_3 < 0.5 \\ w \times F_j - c_1((ub_j - lb_j)c_2 + lb_j) \times s, & c_3 \geq 0.5 \end{cases} \tag{18}$$

where  $c_2$  and  $c_3$  are random number between  $[0, 1]$ .

Improvement of follower position update formula

In the follower position update phase of SSA, the  $i$ th individual will update position according to  $i$ th and  $(i - 1)$ th salp positions. It only depends on the previous



individuals, and lacks learning interaction with other individuals. If the previous follower position is a local optimal solution, the algorithm is prone to fall into a local optimal solution, resulting in stagnation. In addition, the followers updated position for SSA will replace the original individuals regardless of their fitness, which is blind. In order to overcome these shortcomings, the non-uniform Gaussian mutation operator and greedy selection strategy are introduced in the follower position update stage.

As the follower position update only relies on the previous individual and lacks other individual information, the non-uniform Gaussian mutation operator is added on the basis of the original follower position update formula:

$$x_j^k = \frac{1}{2} (x_j^k + x_j^{k-1}) + \Delta(l, GD_j^k) \tag{19}$$

$$\Delta(l, m) = m \left( 1 - r^{(1-l/L)^b} \right) \tag{20}$$

$$GD_j^k = N \left( (F_j - x_j^k), \sigma \right) \tag{21}$$

where  $\Delta(l, GD_j^k)$  is the non-uniform variation step size, a mutation operator that adaptively adjusts the step size through the Gaussian distribution  $GD_j^k$ ;  $r$  is a random number uniformly distributed in  $[0,1]$ ;  $l$  is the current number of iteration;  $b$  is the system parameter that determines the

degree of non-uniformity; Its value is in  $[1, 5]$ . In this paper,  $b$  equals 2.

The introduction of non-uniform Gaussian mutation operator makes the difference between the food source position and the current individual position obey Gaussian distribution. Then the mutation step size is adaptively adjusted. This method can not only ensure that the follower individual has enough vitality, but also fully utilize the information of the food source. It can improve the accuracy of search, and the individual can avoid falling into the local optimum.

Since it is not guaranteed that after the non-uniform Gaussian mutation operator is added, the follower position is better than the original position, thus, a greedy selection strategy is employed to decide whether to update the follower position. If the fitness value of the new position is better than the fitness value of the original position, the new position will be retained, otherwise it will be discarded. The formula is as follows:

$$X(t+1) = \begin{cases} X^*(t), & f[X^*(t)] \leq f[X(t)] \\ X(t), & f[X^*(t)] > f[X(t)] \end{cases} \tag{22}$$

### 4.3 Performance Comparison of Proposed Optimization Algorithm

In order to test the performance of ISSA, the CEC17 test function is used. The test functions include unimodal and multimodal test functions and are minimization problems. ISSA has been run 30 times, and the lowest best, average best, maximum values and standard deviation value are presented in Appendix A. The results are compared with those of SSA algorithm. The number of search agents and maximum generations are selected as 50 and 50, respectively.

According to Appendix A, it can be seen that ISSA has succeeded to find better solutions in the search space and provides minimum fitness and average best values for CEC 17 functions also. ISSA have performed well in getting global minimum values.

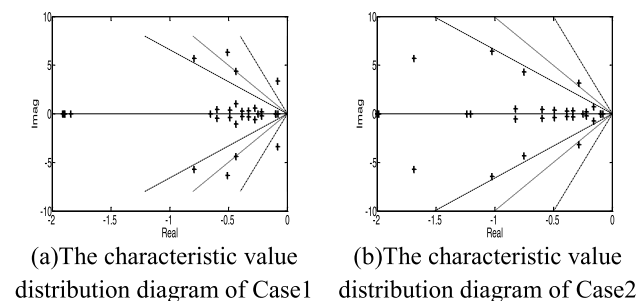


Fig. 8 The characteristic value distribution diagram of system

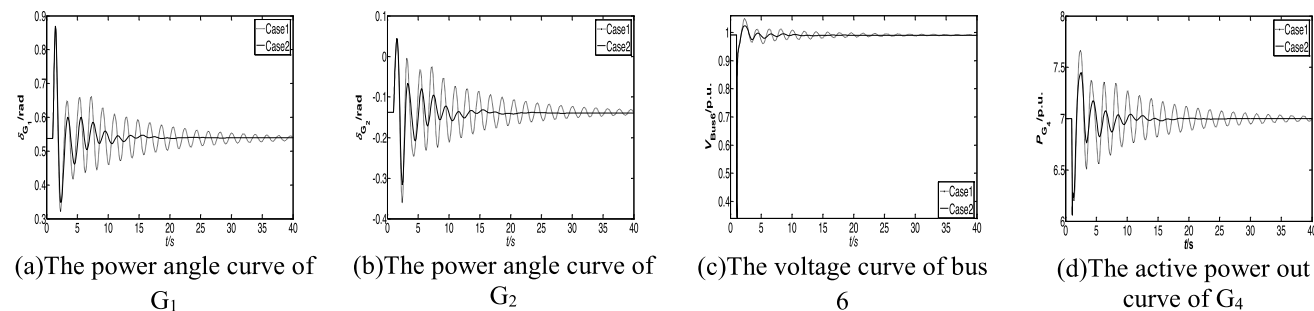


Fig. 9 System response curves of three-phase short circuit

### 4.4 Optimization Process

In this paper, ISSA is used to coordinate and optimize the controller parameters. The number of iteration of the algorithm is set to 50, and the number of population is set to 50. The optimization process is shown in Fig. 6.

The flow chart in Fig. 6 can be explained as follows:

- (1) Initialize the values of the parameters of PSS and TAT-COM-POD,  $K_{PSS}$ ,  $T_{PSS}$ ,  $K_{PSS}$ ,  $T_{PSS}$ ,  $T_{p1}$ ,  $T_{p2}$ ,  $T_{p3}$ ,  $T_{p4}$ ,  $K_p$ ,  $T_p$ ,  $K_c$ ,  $T_c$ ,  $T_1$ ,  $T_2$ ,  $T_3$ ,  $T_4$ , which will be optimized, by generating the initial population of salps with random position.
- (2) Evaluate the objective function (12) to obtain the fitness of all the salps.
- (3) According to the order of fitness, the population positions of salps are sorted, and the best individual is identified as food.

- (4) The leaders and followers positions are updated by formula (18) and (19), (22) respectively.
- (5) Make sure the updated location is better than the previous location.
- (6) Iteration = Iteration + 1.
- (7) Update food location.
- (8) When the algorithm reaches the maximum number of iteration, output parameters, otherwise go to (2).

## 5 Example and Simulation

### 5.1 Parameter Optimization Simulation

The WTB transmission system in Fig. 7 is used in this section. The system includes sending end system and receiving end system, which are connected through AC transmission lines. The sending end system is a WTB transmission

**Table 3** Low-frequency oscillation modes of the system under different transmission power of tie lines

Tie line power / MW	Mode	Case1			Case2			DMs
		$\lambda$	$\xi/\%$	$f/\text{Hz}$	$\lambda$	$\xi/\%$	$f/\text{Hz}$	
250	1	$-0.6083 \pm j6.0755$	9.96	0.9669	$-1.0211 \pm j6.0703$	16.59	0.9661	G <sub>3</sub> ,G <sub>4</sub>
	2	$-0.8186 \pm j5.6779$	14.27	0.9037	$-1.2962 \pm j5.7428$	22.02	0.9140	G <sub>1</sub> ,G <sub>2</sub>
	3	$-0.4254 \pm j4.3735$	9.68	0.6961	$-0.5746 \pm j4.3752$	13.02	0.6963	G <sub>1</sub> ,G <sub>2</sub> ,G <sub>5</sub>
	4	$-0.0573 \pm j3.4428$	1.66	0.5479	$-1.1327 \pm j2.8987$	36.40	0.4613	G <sub>3</sub> ,G <sub>4</sub> ,G <sub>5</sub>
	5	$-0.1722 \pm j0.4582$	35.17	0.0729	$-0.1456 \pm j0.4933$	28.31	0.0785	G <sub>1</sub> -G <sub>5</sub> ,DFIG
298	1	$-0.5601 \pm j6.1799$	9.03	0.9836	$-1.0642 \pm j6.2644$	16.75	0.9970	G <sub>3</sub> ,G <sub>4</sub>
	2	$-0.8067 \pm j5.6858$	14.05	0.9049	$-1.1765 \pm j5.7390$	20.08	0.9134	G <sub>1</sub> ,G <sub>2</sub>
	3	$-0.4274 \pm j4.3767$	9.72	0.6966	$-0.5721 \pm j4.3653$	12.99	0.6948	G <sub>1</sub> ,G <sub>2</sub> ,G <sub>5</sub>
	4	$-0.0789 \pm j3.4157$	2.31	0.5436	$-1.0626 \pm j3.2464$	31.11	0.5167	G <sub>3</sub> ,G <sub>4</sub> ,G <sub>5</sub>
	5	$-0.1833 \pm j0.4753$	35.99	0.0756	$-0.1512 \pm j0.5118$	28.33	0.0815	G <sub>1</sub> -G <sub>5</sub> ,DFIG
344	1	$-0.5276 \pm j6.2582$	8.40	0.9960	$-1.2330 \pm j6.4809$	18.69	1.0315	G <sub>3</sub> ,G <sub>4</sub>
	2	$-0.7984 \pm j5.6850$	13.91	0.9048	$-1.1762 \pm j5.6984$	20.22	0.9069	G <sub>1</sub> ,G <sub>2</sub>
	3	$-0.4304 \pm j4.3725$	9.79	0.6959	$-0.6845 \pm j4.3019$	15.71	0.6847	G <sub>1</sub> ,G <sub>2</sub> ,G <sub>5</sub>
	4	$-0.0963 \pm j3.3745$	2.85	0.5371	$-0.5061 \pm j3.1596$	15.82	0.5029	G <sub>3</sub> ,G <sub>4</sub> ,G <sub>5</sub>
	5	$-0.1948 \pm j0.4899$	36.95	0.0780	$-0.1590 \pm j0.5303$	28.72	0.0844	G <sub>1</sub> -G <sub>5</sub> ,DFIG

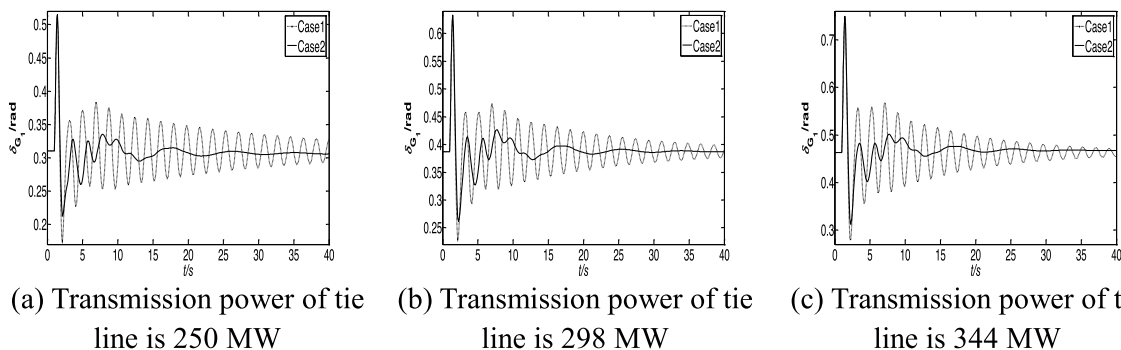


**Fig. 10** Three phase short circuit response curves of the system under different transmission power of tie lines

system, including thermal power units and wind power units. The receiving end system is an IEEE 4-machine 2-area system. The detailed parameters can be seen in the literature [41]. In order to facilitate the analysis, this paper uses the single fan model to replace the lumped model of the wind farm. In order to improve the low-frequency oscillation characteristics of WTB system, five PSSs and one STATCOM-POD controller are installed in the system. In order to improve the stability of the power system, find out the weak bus by calculating the maximum load carrying capacity  $Q_{max}$  of each load bus, as shown in Table 1. The load bus with the minimum maximum load carrying capacity is the weak bus. The STATCOM-POD controller is installed on the bus. In Eq. (10),  $\alpha$  is taken as 1 and  $\beta$  is taken as 5. In objective function (12),  $C_1$  is taken as 1 and  $C_2$  is taken as 0.5.

The meanings of Case1 and Case2 in the following figures and tables are explained as follows: Case1: the system before coordination and optimization of controllers, Case2: the system after coordination and optimization of controllers.

Eigenvalue analysis is performed in the linearized system. Table 2 shows the low-frequency oscillation modes of the system and its eigenvalues, damping, frequency and dominant machines (DMs). By calculating the eigenvalues of  $A$  in Eq. (7), it can be found that compared with the three modes

**Table 4** System low-frequency oscillation modes after increasing the output of wind-thermal-bundled power

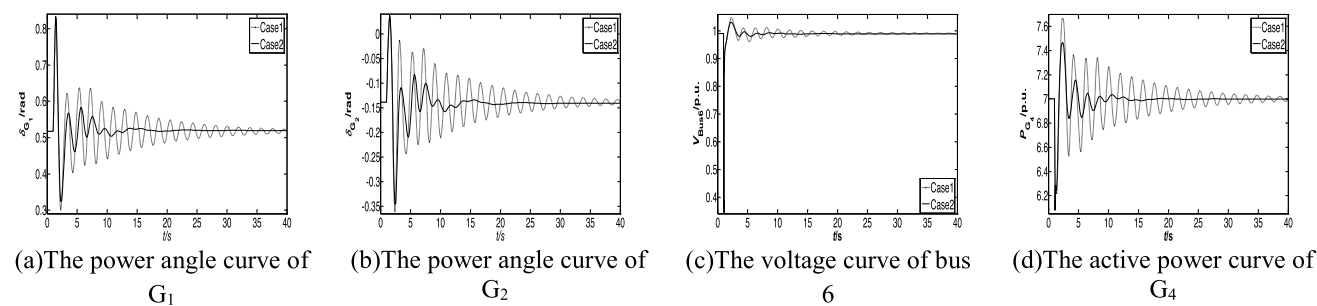
	Mode	$\lambda$	$\xi/\%$	$f/\text{Hz}$	DMs
Case1	1	$-0.5111 \pm j6.3096$	8.07	1.0042	$G_3, G_4$
	2	$-0.7945 \pm j5.6785$	13.86	0.9038	$G_1, G_2$
	3	$-0.4321 \pm j4.3595$	9.86	0.6938	$G_1, G_2, G_5$
	4	$-0.1126 \pm j3.3298$	3.38	0.5300	$G_3, G_4, G_5$
	5	$-0.1927 \pm j0.5271$	34.33	0.0839	$G_1, G_5, \text{DFIG}$
Case2	1	$-1.4052 \pm j6.5912$	20.85	1.0490	$G_3, G_4$
	2	$-1.3157 \pm j5.6800$	22.57	0.9040	$G_1, G_2$
	3	$-0.5621 \pm j4.3306$	12.87	0.6892	$G_1, G_2, G_5$
	4	$-0.4607 \pm j3.1442$	14.50	0.5004	$G_3, G_4, G_5$
	5	$-0.1381 \pm j0.5698$	23.55	0.0907	$G_1, G_5, \text{DFIG}$

of the traditional 4-machine 2-area system, due to the access of WTB sources, the modified power system will add two low-frequency oscillation modes, which will aggravate the oscillation of the system.

According to the DMs in Table 2, mode 1 and mode 2 are the local oscillations of area 1 and area 2 respectively; Mode 3 and mode 4 are both the inter-area oscillations between sending end system and receiving end system. Mode 5 is the inter-area oscillation mode between all units including the wind farms. After optimization, the eigenvalues related to the low-frequency oscillation modes of the system and the corresponding damping ratio have been significantly improved. It can be seen from Table 2 that compared with Case 1, the damping ratios of mode 1, 2, 3 and mode 4 in Case 2 are increased by 95.29%, 104.84%, 74.70%, and 179.82% respectively. Among them, the damping ratio of mode 4 is the smallest. The higher its value of the minimum damping ratio is, the greater the ability to damp low-frequency oscillation for the controller is. This shows that after algorithm optimization, different controllers can be coordinated, so that the proposed controller can better suppress the low-frequency oscillation, which also verifies the effectiveness of the ISSA.

Figure 8 shows the distribution of eigenvalues of the system on the complex plane for Case1 and Case2. The horizontal axis is the real part of the eigenvalue. The vertical axis is the imaginary part of the eigenvalue. The dotted lines from the outside to the inside represent the equivalent damping ratio lines with damping ratios of 5%, 10% and 15% in turn. It can be seen from Fig. 8 that compared with Case 1, the eigenvalue originally outside the line of 5% equal damping ratio left moves inside the line of equal damping ratio. The optimization based on ISSA makes the real part of the system eigenvalue left move on the complex plane. Most of the system eigenvalues in Case2 distribute in the 15% equal damping ratio line, and only one pair of eigenvalues distribute at about 10% equal damping ratio line. The stability of the system is improved.

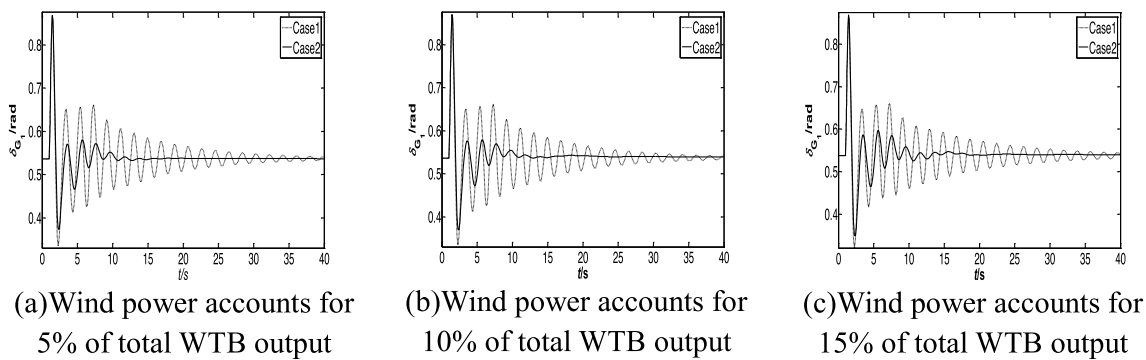
Then time domain simulation is carried out for further analysis. Suppose that a three-phase short circuit fault



**Fig. 11** Three phase short circuit response curves after increasing new energy output

**Table 5** System low-frequency oscillation modes for different proportion of the wind power and thermal power

Percentage of wind power in total output /%	Mode	Case1			Case2			DMs
		$\lambda$	$\xi/\%$	$f/\text{Hz}$	$\lambda$	$\xi/\%$	$f/\text{Hz}$	
5	1	$-0.5111 \pm j6.3094$	8.07	1.0042	$-1.5783 \pm j6.6990$	22.93	1.0662	$G_3, G_4$
	2	$-0.7931 \pm j5.6753$	13.84	0.9032	$-1.0589 \pm j5.6387$	18.46	0.8974	$G_1, G_2$
	3	$-0.4015 \pm j4.3835$	9.12	0.6977	$-0.6772 \pm j4.3116$	15.52	0.6862	$G_1, G_2, G_5$
	4	$-0.1096 \pm j3.3113$	3.31	0.5270	$-0.3888 \pm j3.1044$	12.43	0.4941	$G_3, G_4, G_5$
	5	$-0.2123 \pm j0.3975$	47.11	0.0633	$-0.2171 \pm j0.4184$	46.06	0.0666	$G_1-G_5, \text{DFIG}$
10	1	$-0.5111 \pm j6.3096$	8.07	1.0042	$-1.4669 \pm j6.6619$	21.50	1.0603	$G_3, G_4$
	2	$-0.7932 \pm j5.6758$	13.84	0.9033	$-1.6561 \pm j5.7343$	27.75	0.9126	$G_1, G_2$
	3	$-0.4180 \pm j4.3730$	9.52	0.6960	$-0.7115 \pm j4.3345$	16.20	0.6899	$G_1, G_2, G_5$
	4	$-0.1099 \pm j3.3163$	3.31	0.5278	$-0.4588 \pm j3.0588$	14.83	0.4868	$G_3, G_4, G_5$
	5	$-0.2036 \pm j0.4808$	39.00	0.0765	$-0.1879 \pm j0.4246$	40.47	0.0676	$G_1-G_5, \text{DFIG}$
15	1	$-0.5111 \pm j6.3097$	8.07	1.0042	$-1.1614 \pm j6.4937$	17.61	1.0335	$G_3, G_4$
	2	$-0.7931 \pm j5.6763$	13.84	0.9034	$-1.6048 \pm j5.7098$	27.06	0.9087	$G_1, G_2$
	3	$-0.4355 \pm j4.3603$	9.94	0.6940	$-0.6681 \pm j4.2935$	15.38	0.6833	$G_1, G_2, G_5$
	4	$-0.1104 \pm j3.3211$	3.32	0.5286	$-0.3275 \pm j3.1528$	10.33	0.5018	$G_3, G_4, G_5$
	5	$-0.2081 \pm j0.5060$	38.03	0.0805	$-0.1681 \pm j0.5534$	29.06	0.0881	$G_1-G_5, \text{DFIG}$

**Fig. 12** Three phase short circuit response curves of changing the ratio of wind power and thermal power

occurs in one circuit of double circuit tie lines 7 and 8 when  $t = 1.0$  s. The fault clearing time is 0.1 s. The line is put into operation again when  $t = 1.1$  s. The simulation time is 40 s. The transient response of the system is shown in Fig. 9. The (a) and (b) are the relative power angle curves of between  $G_1$  and  $G_4$  and between  $G_2$  and  $G_3$  respectively. The (c) is the voltage curve of bus 6, and the (d) is the active power out curve of  $G_4$ . As shown in Fig. 9, it can be seen that the oscillation amplitude of the correlation curves decrease.

after parameter optimization, when the system encountered a fault. Furthermore, it can be seen clearly that the oscillation is damped out in about 21 s, 21 s, 12 s and 20 s when using the proposed controllers with optimized parameters, which is quite less when compared with Case1. The transient voltage capability of the system is improved and the voltage oscillation amplitude is reduced during the transient process. The voltage recovery and stability time is faster. This proves that the proposed optimization strategy

is effective in suppressing low-frequency oscillation and reducing the interaction between controllers.

## 5.2 Change Transmission Power of Tie Line

In order to better verify the improvement of stability of WTB system by STATCOM-POD controller, PSS and the proposed optimization algorithm, the simulations of different operating conditions are carried out. The power flow direction, the interconnected location of WTB transmission and the output of WTB transmission are the same as those of Sect. 5.1. By changing the output of SGs set in area 1, tie line transmission power is changed. The influence of different tie line transmission power on low-frequency oscillation modes is studied with the controllers with coordinated optimization parameters.

Table 3 shows the comparison of low-frequency oscillation modes of the system under different tie line power

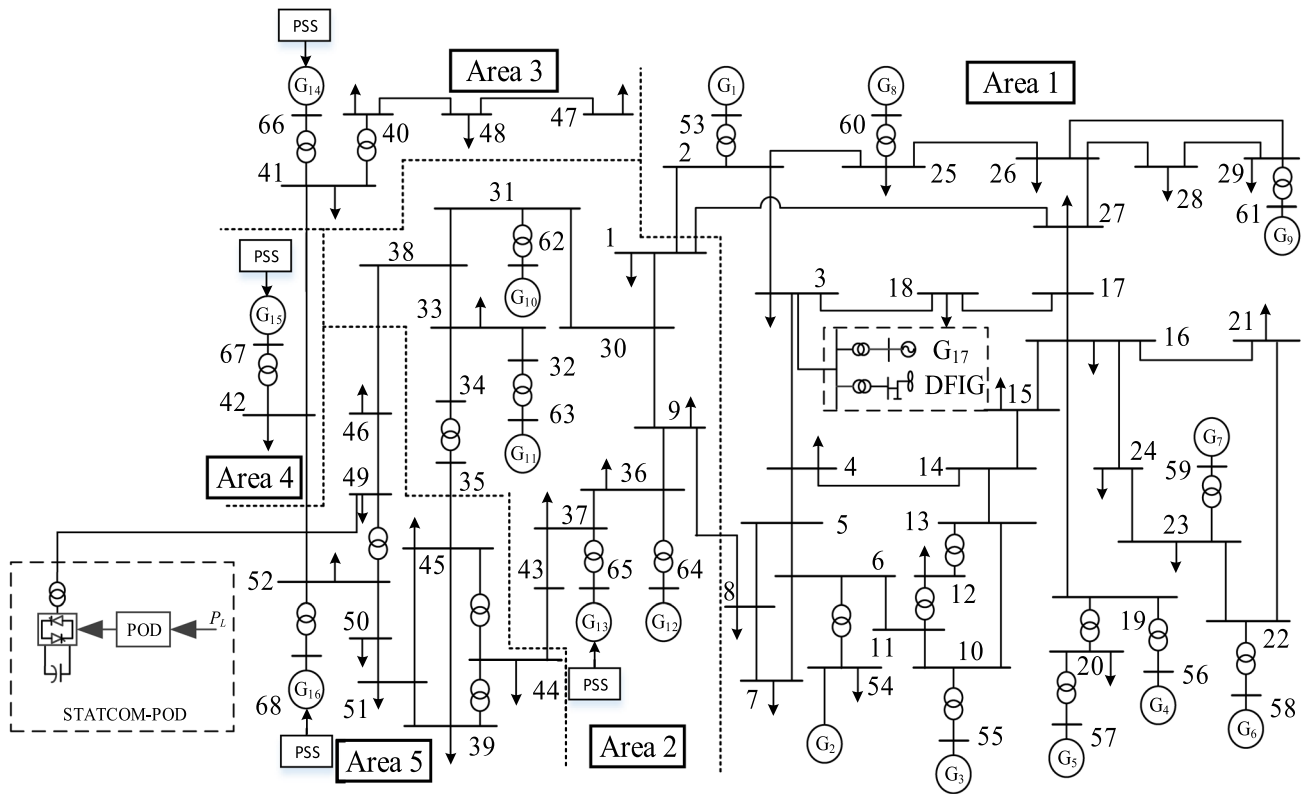


Fig. 13 IEEE 16-machine 68-bus system structure diagram

Table 6 The low-frequency oscillation modes of IEEE 16-machine 68-bus system

Mode	$\lambda$	$\xi/\%$	$f/\text{Hz}$	DMs
1	$-0.4937 \pm j7.6458$	6.44	1.2169	$G_{10}, G_{11}$
2	$-0.9394 \pm j7.0645$	13.18	1.1243	$G_4, G_5$
3	$-0.9122 \pm j6.7616$	13.37	1.0761	$G_6, G_7$
4	$-0.8550 \pm j6.6461$	12.76	1.0578	$G_1, G_8$
5	$-0.3589 \pm j5.8475$	6.13	0.9307	$G_1, G_8, G_9, G_{10}, G_{11}, G_{12}$
6	$-0.5327 \pm j5.9548$	8.91	0.9477	$G_2, G_3$
7	$-0.4050 \pm j5.6038$	7.21	0.8919	$G_1, G_8, G_9, G_{10}, G_{12}, G_{13}$
8	$-0.3309 \pm j5.4254$	6.09	0.8635	$G_1, G_3, G_8, G_9, G_{10}, G_{12}, G_{13}$
9	$-0.6285 \pm j5.0523$	12.34	0.8041	$G_4, G_5, G_6, G_7$
10	$-0.3910 \pm j4.7433$	8.22	0.7549	$G_2, G_3, G_9$
11	$-0.3531 \pm j4.4267$	7.95	0.7045	$G_1, G_4, G_5, G_6, G_7, G_8, G_9$
12	$-0.1496 \pm j3.1491$	4.74	0.5012	$G_{12}, G_{13}, G_{14}, G_{15}, G_{16}$
13	$-0.1753 \pm j2.8983$	6.04	0.4613	$G_4, G_5, G_6, G_7, G_9, G_{12}, G_{13}, G_{14}, G_{15}, G_{16}$
14	$-0.1292 \pm j2.3707$	5.44	0.3773	$G_{14}, G_{15}, G_{16}, G_{17}$
15	$-0.1775 \pm j2.0518$	8.62	0.3265	$G_{13}, G_{14}, G_{16}, G_{17}$
16	$-0.1273 \pm j1.5436$	8.22	0.2457	$G_{12}, G_{13}, G_{14}, G_{15}, G_{17}$
17	$-0.1335 \pm j0.2594$	45.77	0.0413	$G_1-G_{17}, \text{DFIG}$

flows. With the change of transmission power of tie lines, the damping ratios of low-frequency oscillation modes change. By comparing the system damping ratios before optimizing the controller parameters with those after optimization, it can be found that the system damping ratios have been

improved and the system damping characteristics have been enhanced after optimization.

It is assumed that the system has the same short circuit fault as described in Sect. 5.1. Figure 10 depicts the comparative response curve of  $G_1$  relative power angle. By

**Table 7** The characteristic root comparison of IEEE 16-machine 68-bus system before and after optimization

	Mode	$\lambda$	$\xi/\%$	$f/\text{Hz}$	DMs
Case1	12	$-0.1531 \pm j3.1456$	4.86	0.5006	$G_{12}, G_{13}, G_{14}, G_{15}, G_{16}$
	13	$-0.1764 \pm j2.9017$	6.07	0.4618	$G_4, G_5, G_6, G_7, G_9, G_{12}, G_{13}, G_{14}, G_{15}, G_{16}$
	14	$-0.1296 \pm j2.3676$	5.46	0.3768	$G_{14}, G_{15}, G_{16}, G_{17}$
	15	$-0.1778 \pm j2.0527$	8.63	0.3267	$G_{13}, G_{14}, G_{16}, G_{17}$
	16	$-0.1284 \pm j1.5494$	8.26	0.2466	$G_{12}, G_{13}, G_{14}, G_{15}, G_{17}$
Case2	12	$-0.2063 \pm j3.1318$	6.57	0.4984	$G_{12}, G_{13}, G_{14}, G_{15}, G_{16}$
	13	$-0.1934 \pm j2.8932$	6.67	0.4605	$G_4, G_5, G_6, G_7, G_9, G_{12}, G_{13}, G_{14}, G_{15}, G_{16}$
	14	$-0.1731 \pm j2.3528$	7.34	0.3745	$G_{14}, G_{15}, G_{16}, G_{17}$
	15	$-0.1806 \pm j2.0508$	8.77	0.3264	$G_{13}, G_{14}, G_{16}, G_{17}$
	16	$-0.1496 \pm j1.5348$	9.70	0.2443	$G_{12}, G_{13}, G_{14}, G_{15}, G_{17}$

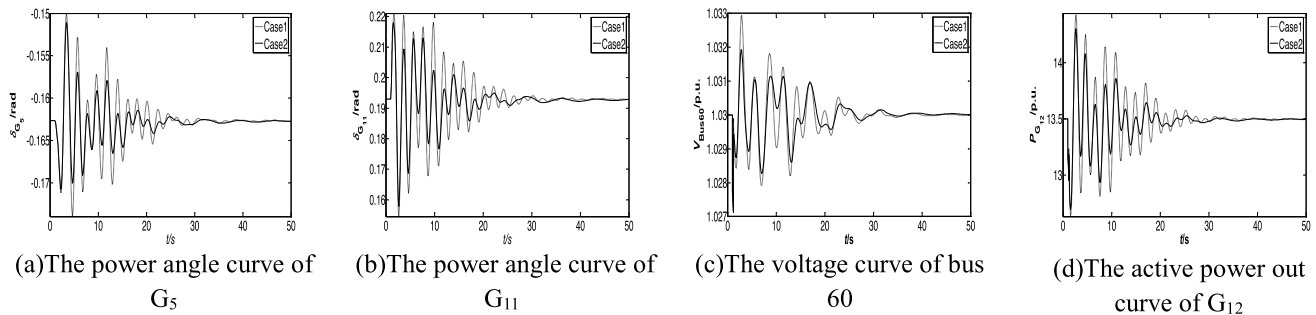


**Fig. 14** Three phase short circuit response curves of IEEE 16-machine 68-bus system

comparing (a), (b) and (c) in Fig. 10, it can be observed that with the increase of transmission power of tie lines, the oscillation amplitude of the relevant curves gradually increases. It takes more time to stabilize.

After optimizing the controller parameters, the maximum oscillation amplitude and stabilization time of the system decrease. This shows that the coordination and optimization method of controller parameters based on ISSA can provide sufficient damping for WTB transmission system and effectively improve the stability of the system. The optimized controller parameters can improve the stability of the system even if the transmission power of the tie line changes.

### 5.3 Increase the Output of Wind Power

The operating condition of this section is to increase the wind power output while keeping the transmission power of tie lines unchanged. The wind power output is increased by 40%. This section studies the performance of the proposed.

optimization strategy under this operating condition.

Table 4 shows the low-frequency oscillation modes of the system after the wind power output power is increased by 40%. After algorithm optimization, compared with Case1, the damping ratios of the system are improved.

The damping ratios of mode 1, 2, 3 and 4 are increased by 158.36%, 63.20%, 30.53% and 328.99% respectively.

As shown in Fig. 11, when the same fault as Sect. 5.1 occurs, the coordinated and optimized controllers can still better suppress oscillation. The curves of relative power angle of  $G_1$  and  $G_2$ , the voltage of bus 6 and the output active power of  $G_4$  are improved to varying degrees. The optimized system tends to be stable at about 18 s, about 22 s earlier than the original system, shortening the time to return to stability. This also shows that the proposed method can still suppress system oscillation and improve system stability under the operating condition of this section.

### 5.4 Change the Ratio of Wind Power and Thermal Power

The operating condition of this section is to change the ratio of wind power and thermal power while keeping the output power of WTB unchanged. This section studies the performance of the proposed optimization strategy under this operating condition.

Table 5 shows the low-frequency oscillation modes of system after changing the ratio of wind power and thermal power. By coordinating and optimizing the controllers, the damping ratios of modes 1, 2, 3 and 4 are improved to varying degrees.

Set the same short circuit fault as Sect. 5.1. Figure 12 shows the comparative response curve of  $G_1$  relative power angle. By comparing (a), (b) and (c) in Fig. 12, it can be seen that the controllers optimized by ISSA can better decrease the oscillation amplitude of the correlation curves and shorten the time to return to the steady state. This shows that the proposed optimization strategy is still effective under the operating condition of this section.

### 5.5 IEEE 16-Machine 68-Bus System

In order to verify the effectiveness of the algorithm in large power system, the proposed algorithm is tested in more complex networks. The simulation is carried out on the interconnected New York Power System and New England Transmission System (NYPS-NETS). As is shown in Fig. 13, the structure of the NYPS-NETS consists of 16 SGs.  $G_1$ - $G_9$  are in New England and  $G_{10}$ - $G_{16}$  in New York and its neighborhood. The WTB transmission system is connected to bus 3. The system can transmit the electric energy generated by the new energy unit to the remote place via the transmission line. The SG  $G_{17}$  is newly added. The output of wind power and thermal power is 50 MW and 220 MW respectively. The SGs are the fourth order model described above and are equipped with AVR and TG. The detailed system parameters can be referred to the literature [42, 43].

Table 6 shows the low-frequency oscillation modes of the interconnection system. In Table 6, the damping ratios of modes 12, 13, 14, 15 and 16 are generally small, and they are inter regional oscillation modes. The oscillation modes are strongly correlated with  $G_{13}$ ,  $G_{14}$ ,  $G_{15}$  and  $G_{16}$ . This paper chooses to add PSS to  $G_{13}$ ,  $G_{14}$ ,  $G_{15}$  and  $G_{16}$  to better enhance the damping characteristics of the system. By calculating the maximum load carrying capacity of each load bus, the results show bus 49 has the minimum maximum load carrying capacity. The calculation results can be seen in Appendix B. The STATCOM-POD controller is connected to bus 49. The active power  $P_L$  from bus 49 to bus 52 is selected as the controller input signal.

By Tables 6 and 7, it can be found that the damping ratios of some modes are improved to some extent after installing PSS and STATCOM-POD controllers. It can be seen from Table 7 that the damping ratios of oscillation modes are improved after coordinating and optimizing the controllers.

Assume that the fault occurs at bus 52. Figure 14 shows the corresponding response curves. The fault time is  $t_s = 1.0$  s, and the fault duration is 0.2 s. After parameters are coordinated and optimized, the oscillation amplitude of the relative power angle, active power output and voltage of the bus is reduced. The time to restore stability is also shortened. This also verifies the effectiveness of the proposed optimization algorithm for large power system.

## 6 Conclusion

This paper presents a coordination and optimization strategy of PSS and STATCOM-POD in WTB system based on ISSA. The purpose is to suppress the low-frequency oscillation phenomenon in WTB system and reduce the interaction between controllers. The simulation of various operating conditions is carried out in IEEE 4-machine 2-area system. It also carried out in the IEEE 16-machine 68-bus system. The results of eigenvalue analysis and time domain simulation verify the effectiveness of the proposed control strategy. The main conclusions are as follows:

1. A new optimization algorithm named ISSA is proposed, which has been developed as the solution technique for coordination and optimization design of PSS and STATCOM-POD. It is thoroughly investigated for different operating conditions.
2. The CEC17 test function results show that introducing the adaptive weight factor, Levy flight disturbance strategy, non-uniform Gaussian mutation operator and greedy selection strategy for SSA is conducive to overcoming local convergence problem and improving accuracy of controller parameters optimization.
3. For the proposed controllers coordination and optimization problem, the real part and damping ratio of low-frequency oscillation mode and bus voltage are taken as the objective function to improve the damping characteristics of WTB system and suppress the low-frequency oscillation of the system. The simulation results show that the coordinated design of PSS and STATCOM-POD parameters can effectively eliminate the adverse effects between different controllers to achieve the optimal control effect. Under the different operating conditions, the oscillation amplitude and the time required to stabilize for the system are also significantly shortened.
4. The proposed coordination and optimization design is robust and simple to implement.

The further work is the application of the proposed algorithm to solve the stability problem of WTB system while considering system economics such as installation cost, network loss and etc. The coordination between multiple FACTS-POD and power system stabilizers is the future scope of this work.

## Appendix A

See Table 8.

**Table 8** Comparison of test function results

Name of the function	ISSA				SSA			
	Maximum value	Minimum value	Average value	Standard deviation value	Maximum value	Minimum value	Average Value	Standard deviation value
Bent Cigar function	6.57e−04	1.69 e−04	3.71e−04	1.30e−04	3.33e+09	7.94e+08	1.80e+09	6.29e+08
Sum of Different Power function	7.25e−27	9.28e−31	1.23e−27	1.92e−27	2.48e−12	1.06e−15	3.85e−13	6.37e−13
Zakharov function	2.42e−09	8.50e−10	1.42e−09	4.14e−10	7.42e+03	1.72e+03	3.93e+03	1.38e+03
Rosenbrock’s function	2.90e+01	2.89e+01	2.90e+01	1.84e−02	7.47e+07	5.11e+06	3.26e+07	1.69e+07
Rastrigin’s function	3.48e+02	7.78e+01	2.38e+02	5.00e+01	3.74e+03	9.58e+02	2.27e+03	6.03e+02
Levy function	2.88e+01	2.73	4.23	4.57	1.14e+03	3.44e+02	6.88e+02	2.17e+02
High Conditioned Elliptic function	8.57e−06	1.51e−06	3.92e−06	1.69e−06	7.55e+07	3.98e+06	2.86e+07	1.65e+07
Discus function	2.30e−08	4.11e−09	1.01e−08	4.13e−09	8.66e+04	4.05e+03	1.68e+04	1.54e+04
Weierstrass function	1.58e−10	1.01e−11	2.90e−11	2.90e−11	1.81	1.26	1.47	1.40e−01
HappyCat function	1.43	6.99e−01	1.06	1.57e−01	7.10e+01	1.81e+01	3.76e+01	1.19e+01

## Appendix B

See Table 9

**Table 9** Ranking of load bus maximum load carrying capacity

	$Q_{max}$ (p.u.)	Bus	$Q_{max}$ (p.u.)	Bus	$Q_{max}$ (p.u.)	Bus	$Q_{max}$ (p.u.)	Bus	$Q_{max}$ (p.u.)	Bus	$Q_{max}$ (p.u.)	Bus	$Q_{max}$ (p.u.)
49	189.1	28	467.0	17	691.2	19	737.5	6	931.3	31	1178.4	52	4979.5
25	209.9	26	471.9	16	709.2	7	773.6	14	931.9	39	1229.4	42	7208.7
48	277.3	27	522.9	51	710.3	3	773.9	11	943.8	9	1238.3	37	9185.5
46	283.3	34	541.7	18	713.9	21	804.5	4	944.7	22	1431.7	41	12,243.4
40	287.9	29	589.6	8	728.2	1	834.9	13	945.9	44	1500.1		
47	341.3	20	609.7	24	728.9	23	890.2	33	970.9	43	1582.7		
2	400.9	15	639.7	38	729.0	5	894.1	10	1038.1	32	1615.9		
12	413.3	35	642.1	45	735.9	50	914.0	30	1143.6	36	3100.5		



**Acknowledgements** The work is jointly supported by the National Natural Science Foundation of China (No. 52377125), the Scientific and Technological Research Foundation of Henan Province (No. 222102320198), and the Key Project of Zhengzhou University of Light Industry (2020ZDPY0204).

## Declarations

**Conflict of interest** The authors have no competing interests to declare that are relevant to the content of this article.

## References

- Razmjoo A, Kaigutha LG, Rad MV, Marzband M, Davarpanah A, Denai M (2021) A Technical analysis investigating energy sustainability utilizing reliable renewable energy sources to reduce CO<sub>2</sub> emissions in a high potential area. *Renew Energy* 164:46–57
- Li Z, Luan R, Lin B (2022) The trend and factors affecting renewable energy distribution and disparity across countries. *Energy* 254:124265
- Sun Y, Dong J (2019) Selection of desirable transmission power mode for the bundled wind-thermal generation systems. *J Clean Prod* 216:585–596
- Xiang L, Zhu HW, Zhang Y, Yao QT, Hu AJ (2022) Impact of Wind Power Penetration on Wind–Thermal–Bundled Transmission System. *IEEE Trans Power Electron* 37(12):15616–15625
- Li J, Li F, et al (2021) Analysis of improving transient stability of DFIG-type wind-thermal binding system by current-limiting SSSC. *Proc CSU-EPSA* 33(05): 68–76 (in Chinese). <https://doi.org/10.19635/j.cnki.csu-epsa.000557>
- He P, Wen F, Ledwich G, Xue Y (2016) An investigation on inter-area mode oscillations of interconnected power systems with integrated wind farms. *Int J Electr Power Energy Syst* 78:148–157
- Bhukya J, Mahajan V (2019) Mathematical modelling and stability analysis of PSS for damping LFOs of wind power system. *IET Renew Power Gener* 13(1):103–115
- Abd-Elazim SM, Ali ES (2012) Coordinated design of PSSs and SVC via bacteria foraging optimization algorithm in a multimachine power system. *Int J Electr Power Energy Syst* 41(1):44–53. <https://doi.org/10.19635/j.cnki.csu-epsa.000557>
- Du W, Dong W, Wang Y, Wang H (2020) A method to design power system stabilizers in a multi-machine power system based on single-machine infinite-bus system model. *IEEE Trans Power Syst* 36(4):3475–3486
- Zhang G, Hu W, Zhao J, Cao D, Chen Z, Blaabjerg F (2021) A novel deep reinforcement learning enabled multi-band pss for multi-mode oscillation control. *IEEE Trans Power Syst* 36(4):3794–3797
- Yu G, Lin T, Zhang J, Tian Y, Yang X (2019) Coordination of PSS and FACTS damping controllers to improve small signal stability of large-scale power systems. *CSEE J Power Energy Syst* 5(4):507–514
- Ali ES, Abd-Elazim SM (2012) Coordinated design of PSSs and TCSC via bacterial swarm optimization algorithm in a multimachine power system. *Int J Electr Power Energy Syst* 36(1):84–92
- Chi Y, Xu Y, Zhang R (2020) Many-objective robust optimization for dynamic var planning to enhance voltage stability of a wind-energy power system. *IEEE Trans Power Delivery* 36(1):30–42
- Biswas S, Nayak PK, Pradhan G (2021) A dual-time transform assisted intelligent relaying scheme for the STATCOM-compensated transmission line connecting wind farm. *IEEE Syst J* 16(2):2160–2171
- Abd-Elazim SM, Ali ES (2016) Imperialist competitive algorithm for optimal STATCOM design in a multimachine power system. *Int J Electr Power Energy Syst* 76:136–146
- Zhang G, Hu W, Cao D, Yi J, Huang Q, Liu Z, Blaabjerg F et al (2020) A data-driven approach for designing STATCOM additional damping controller for wind farms. *Int J Electr Power Energy Syst* 117:105620
- Abd Elazim SM, Ali ES (2016) Optimal SSSC design for damping power systems oscillations via gravitational search algorithm. *Int J Electr Power Energy Syst* 82:161–168
- Kamarposhti MA, Colak I, Iwendi C, Band SS, Ibeke E (2022) Optimal coordination of PSS and SSSC controllers in power system using ant colony optimization algorithm. *J Circ Syst Comput* 31(04):2250060
- Abd Elazim SM, Ali ES (2016) Optimal power system stabilizers design via cuckoo search algorithm. *Int J Electr Power Energy Syst* 75:99–107
- Karuppiah N, Malathi V (2016) Damping of power system oscillations by tuning of PSS and SVC using particle swarm optimization. *Tech Gazette* 23(1):221–227
- Dey P, Mitra S, Bhattacharya A, Das P (2019) Comparative study of the effects of SVC and TCSC on the small signal stability of a power system with renewables. *J Renew Sustain Energy* 11(3):033305
- Zhang H, Feng Y, Huang W, Zhang J, Zhang J (2021) A novel mutual aid Salp Swarm Algorithm for global optimization. *Concurr Comput: Pract Exper* e6556
- Duan Q, Wang L, Kang H, Shen Y, Sun X, Chen Q (2021) Improved salp swarm algorithm with simulated annealing for solving engineering optimization problems. *Symmetry* 13(6):1092
- Sekhane H, Labeled D (2019) Identification of the weakest buses to facilitate the search for optimal placement of var sources using “Kessel and Glavitch” Index. *J Electr Eng Technol* 14(4):1473–1483
- Aydin F, Gümüş B (2022) Comparative analysis of multi-criteria decision making methods for the assessment of optimal SVC location. *Bull Polish Acad Sci: Tech Sci* 70(2):e140555
- Li W, Chao P, Liang X, Ma J, Xu D, Jin X (2017) A practical equivalent method for DFIG wind farms. *IEEE Trans Sustain Energy* 9(2):610–620
- Shabani HR, Kalantar M (2021) Real-time transient stability detection in the power system with high penetration of DFIG-based wind farms using transient energy function. *Int J Electr Power Energy Syst* 133:107319
- He P, Wen F, Ledwich G, Xue Y, Huang J (2015) Investigation of the effects of various types of wind turbine generators on power-system stability. *J Energy Eng* 141(3):1–10
- Kamel OM, Abdelaziz AY, Zaki Diab AA (2020) Damping oscillation techniques for wind farm DFIG integrated into inter-connected power system. *Electr Power Comp Syst* 48(14–15):1551–1570
- Miotto EL, de Araujo PB, de Vargas Fortes E, Gamino BR, Martins LFB (2018) Coordinated tuning of the parameters of PSS and POD controllers using bioinspired algorithms. *IEEE Trans Ind Appl* 54(4):3845–3857
- Kar MK, Kumar S, Singh AK, Panigrahi S (2021) A modified sine cosine algorithm with ensemble search agent updating schemes for small signal stability analysis. *Int Trans Electr Energy Syst* 31(11):e13058
- Chau TK, Yu SS, Fernando T, Iu HHC, Small M (2017) A load-forecasting-based adaptive parameter optimization strategy of STATCOM using ANNs for enhancement of LFOD in power systems. *IEEE Trans Industr Inf* 14(6):2463–2472
- Bhukya J, Mahajan V (2020) Optimization of controllers parameters for damping local area oscillation to enhance the stability

- of an interconnected system with wind farm. *Int J Electr Power Energy Syst* 119:105877
34. Du W, Bi J, Cao J, Wang HF (2015) A method to examine the impact of grid connection of the DFIGs on power system electromechanical oscillation modes. *IEEE Trans Power Syst* 31(5):3775–3784
  35. Dey P, Saha A, Bhattacharya A, Marungsri B (2020) Analysis of the effects of PSS and renewable integration to an inter-area power network to improve small signal stability. *J Electr Eng Technol* 15(5):2057–2077
  36. Mehta B, Bhatt P, Pandya V (2015) Small signal stability enhancement of DFIG based wind power system using optimized controllers parameters. *Int J Electr Power Energy Syst* 70:70–82
  37. Bian XY, Geng Y, Lo KL, Fu Y, Zhou QB (2015) Coordination of PSSs and SVC damping controller to improve probabilistic small-signal stability of power system with wind farm integration. *IEEE Trans Power Syst* 31(3):2371–2382
  38. Surinkaew T, Ngamroo I (2014) Coordinated robust control of DFIG wind turbine and PSS for stabilization of power oscillations considering system uncertainties. *IEEE Trans Sustain Energy* 5(3):823–833
  39. Chen ZY, Zhang DM, Xin ZY (2022) Multi-subpopulation based symbiosis and non-uniform gaussian mutation salp swarm algorithm. *Acta Automatica Sinica* 48(5):1307–1317 (in Chinese). <https://doi.org/10.16383/j.aas.c190684>
  40. Iacca G, dos Santos Junior VC, de Melo VV (2021) An improved Jaya optimization algorithm with Lévy flight. *Expert Syst Appl* 165:113902
  41. Kunder P, Balu NJ, Lauby MG (1994) *Power system stability and control*. McGraw-Hill, New York
  42. Pal B, Chaudhuri B (2006) *Robust control in power systems*. Springer, New York
  43. Bento ME, Ramos RA (2020) A method based on linear matrix inequalities to design a wide-area damping controller resilient to permanent communication failures. *IEEE Syst J* 15(3):3832–3840

**Publisher's Note** Springer Nature remains neutral with regard to jurisdictional claims in published maps and institutional affiliations.

Springer Nature or its licensor (e.g. a society or other partner) holds exclusive rights to this article under a publishing agreement with the

author(s) or other rightsholder(s); author self-archiving of the accepted manuscript version of this article is solely governed by the terms of such publishing agreement and applicable law.

**Ping He** She received her B.E. and M.E. degrees from Zhengzhou University, China, in 2003 and 2006, respectively, and Ph.D. from South China University of Technology, China, in 2014, all in electrical engineering. She is currently a Professor with the School of Electrical and Information Engineering, Zhengzhou University of Light Industry, Zhengzhou, China. Her research interests lie in power system stability analysis and control, as well as wind power generation.

**Lei Yun** He was born in Zhengzhou, Hennan, China, in 1996. He is currently pursuing the M.E. degree in electrical engineering at Zhengzhou University of Light Industry, Zhengzhou, China. His research interests include the small signal stability of renewable energy systems.

**Yukun Tao** He received the Ph.D. degree from the School of Electric Power Engineering, South China University of Technology, China, in 2016. Now he is a lecturer in Zhengzhou University of Light Industry, China. His main research interests include power system analysis and control and new energy grid connection.

**Jiale Fan** She received the Ph.D. degree from the School of Electrical Engineering, Southwest Jiaotong University, in 2020. Now she is a lecturer in Zhengzhou University of Light Industry, China. Her main research interests include research on operation optimization and resilience of integrated energy system.

**Zhiwen Pan** He was born in Xuchang, Hennan, China, in 1999. He is currently pursuing the M.E. degree in electrical engineering at Zhengzhou University of Light Industry, Zhengzhou, China. His research interests include the small signal stability of renewable energy systems.

**Mingyang Wang** He was born in Pingdingshan, Hennan, China, in 1999. He is currently pursuing the M.E. degree in electrical engineering at Zhengzhou University of Light Industry, Zhengzhou, China. His research interests include the energy storage modeling and frequency stability research.